Ultrahigh-energy cosmic Rays and neutrinos

A. Kusenko (UCLA)

- Cosmic rays beyond GZK cutoff
- many proposed explanations invoke sources of energetic photons
- neutrinos with $E_\nu \sim 10^{18}$ eV as signature of UHE photons at high red shift

A.K, Postma, hep-ph/0007246

Greisen-Zatsepin-Kuzmin cutoff.

Cosmic-ray protons interact with $T = 2.7\,K$ CMBR photons.

Pion photoproduction (starting at Δ-resonance: $p\gamma \to \Delta^* \to N\pi$)

$$m(\Delta) = 1.232 \text{ GeV}$$

$$s \approx m_p^2 + 2 E_\gamma p_p = m^2(\Delta)$$

$$\Downarrow$$

$$\boxed{p_p \sim 10^{20} \text{ eV}}$$

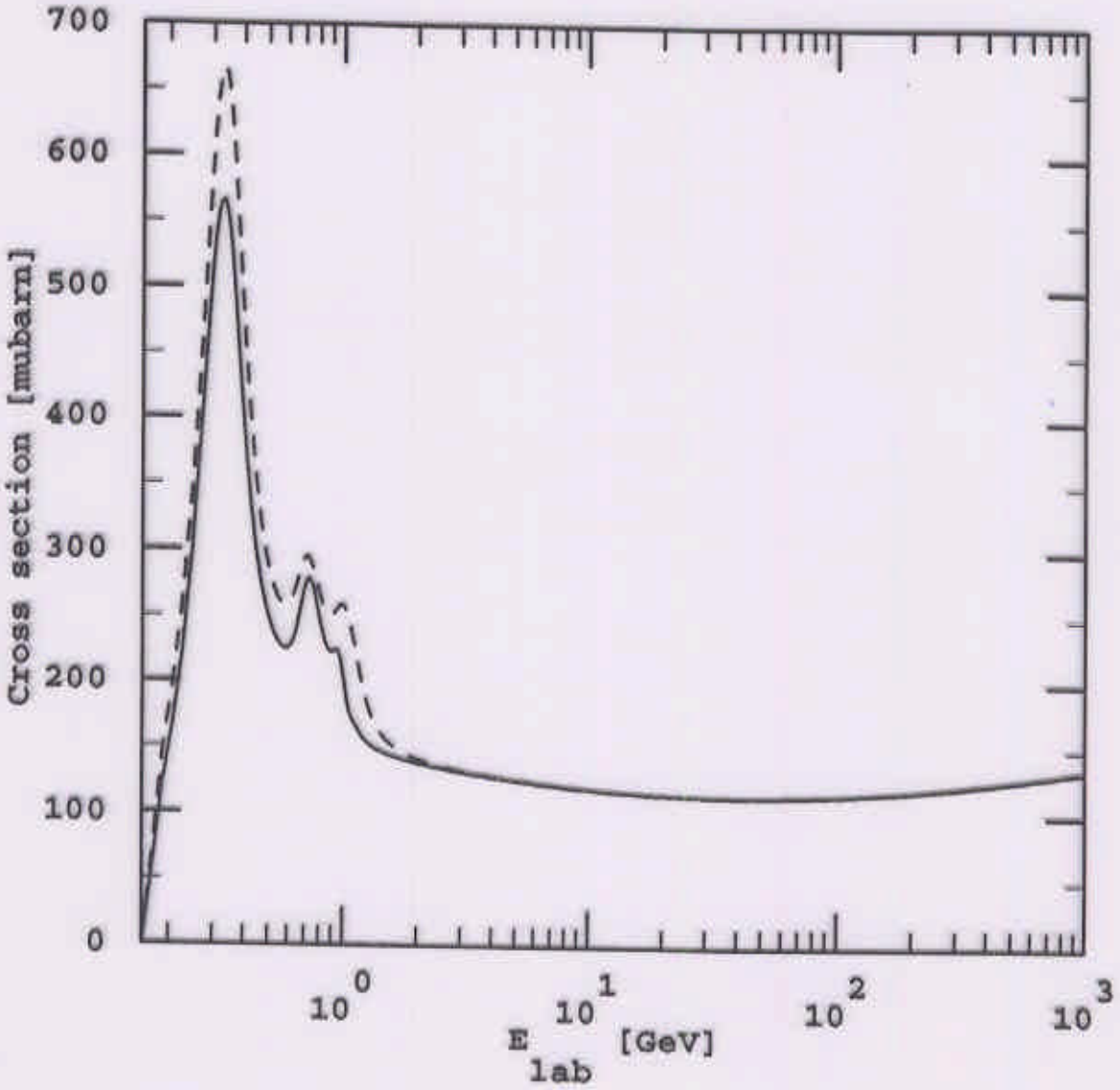

Figure 8: The total photo-pion production cross section for protons (solid line) and neutrons (dashed line).

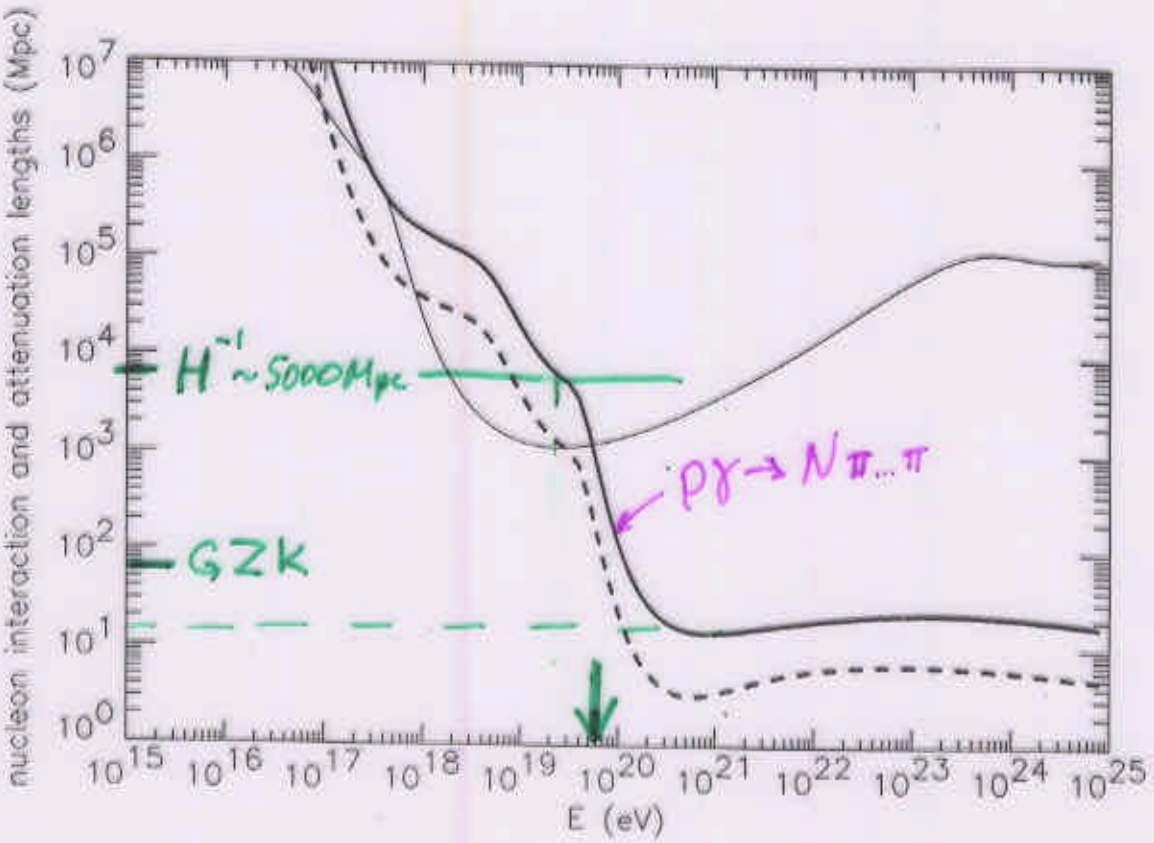

Figure 9: The nucleon interaction length (dashed line) and attenuation length (solid line) for photo-pion production and the proton attenuation length for pair production (thin solid line) in the CMB and the observational estimate of the total extragalactic radio background intensity shown in Fig. 10 below.

PHOTONS: $\gamma\, \gamma_{Radio} \to e^+ e^-$

$\left(\frac{R_{GZK}}{H^{-1}}\right)^3 \sim 10^{-2}$ reduction in volume for $E \geq E_{GZK} \sim 10^{20}$ eV

Penetration depth of photons

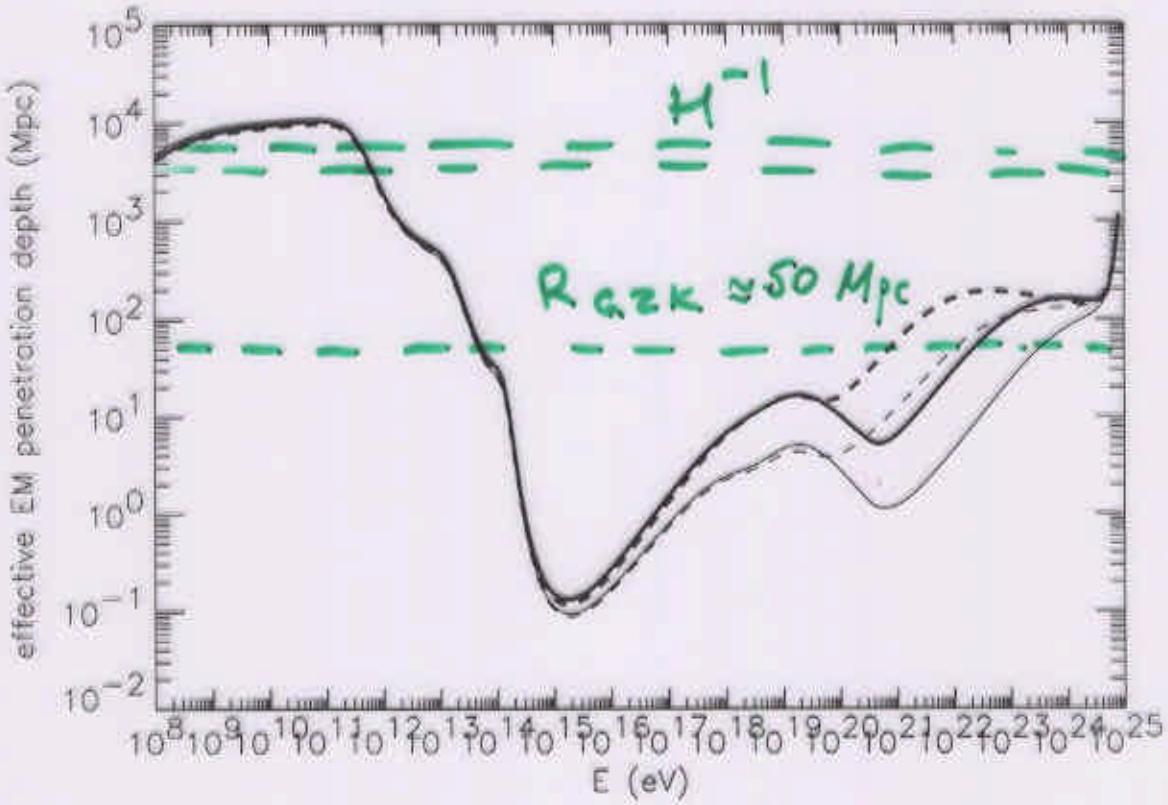

Figure 14: Effective penetration depth of EM cascades, as defined in the text, for the strongest theoretical URB estimate (solid lines), and the observational URB estimate from Ref. [173] (dashed lines), as shown in Fig. 10, and for an EGMF $\ll 10^{-11}$ G (thick lines), and 10^{-9} G (thin lines), respectively.

5

Cosmic Rays

Energy Spectrum of Cosmic Rays

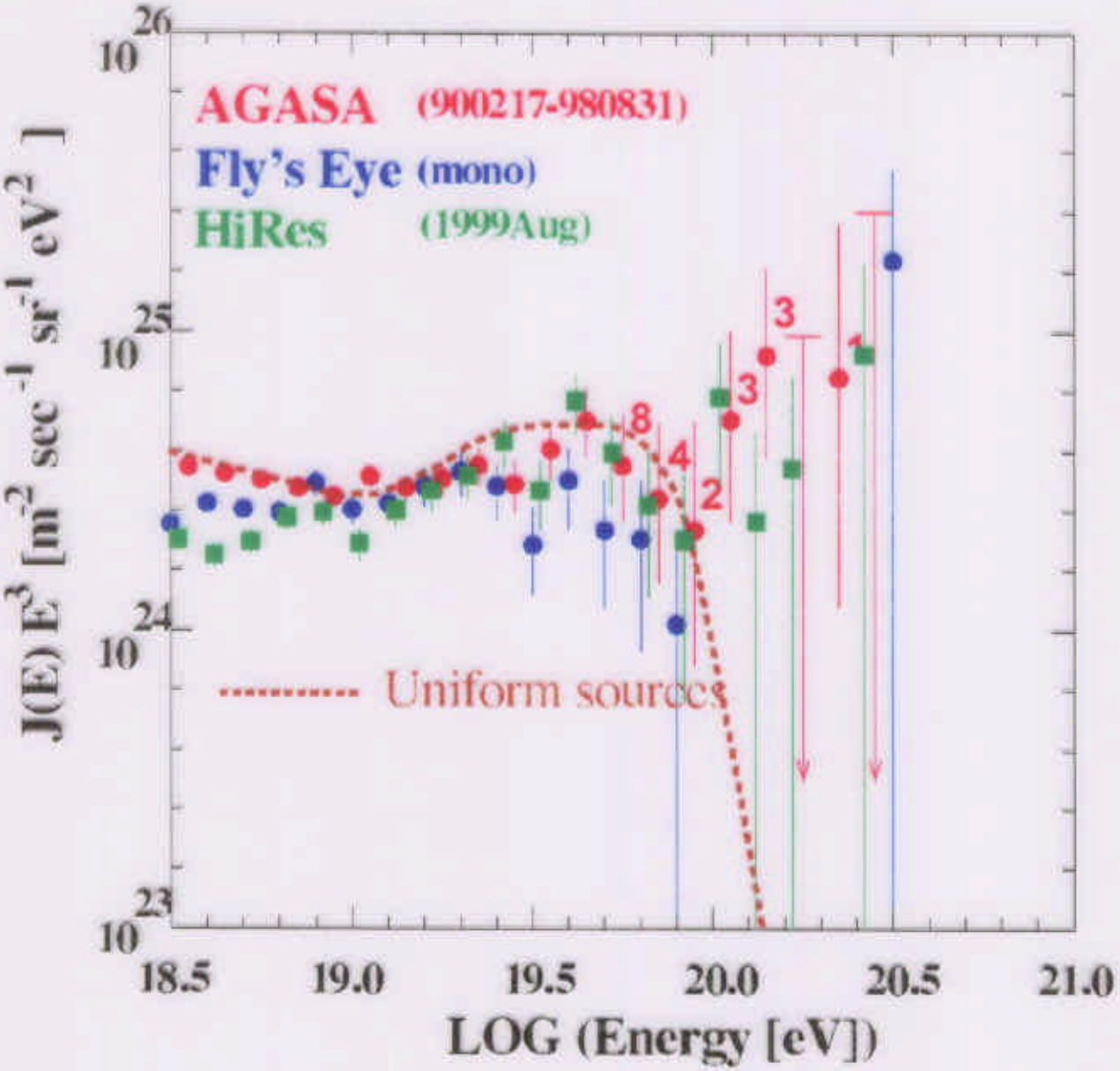

Proposed explanations

"Astrophysical" sources

GRB
Magnetars
AGN
⋮

- exist at $z \lesssim$ few
- accelerate charged particles

⇒ UHECR = protons

"New" sources

Topological defects
relic particles
⋮

- exist at $z \sim 1$ and $z \gg 1$
- UHECR = mainly photons

Can tell the difference?

Present data consistent with p or γ.

At red shift $z \gtrsim 3$

- CMBR has higher temperature ($\gamma\gamma_{CMB} \to \mu^+\mu^-$)
- RB has lower density (less absorption)

⇓

VHE photons produce neutrinos from μ, π decays

⇓

signature of photon sources (TD, relics, etc.)

(A.K, Postma, hep-ph/0007246)

At present, the main source of opacity for photons is universal radio background (RB)

$\gamma\,\gamma_{RB} \rightarrow e^+e^-$ (pair production)

$\sim 10^{20}$ eV

$e\,\gamma_{CMB} \rightarrow e\,\gamma$ (inverse Compton)

fast

high energy

Radio background is produced by normal galaxies + radio galaxies.

At $z > 1$, radio background density is lower (fewer sources; none at $z \sim 10$!)

CMBR has the same comoving density

At $z > z_R \approx 3$, can neglect RB

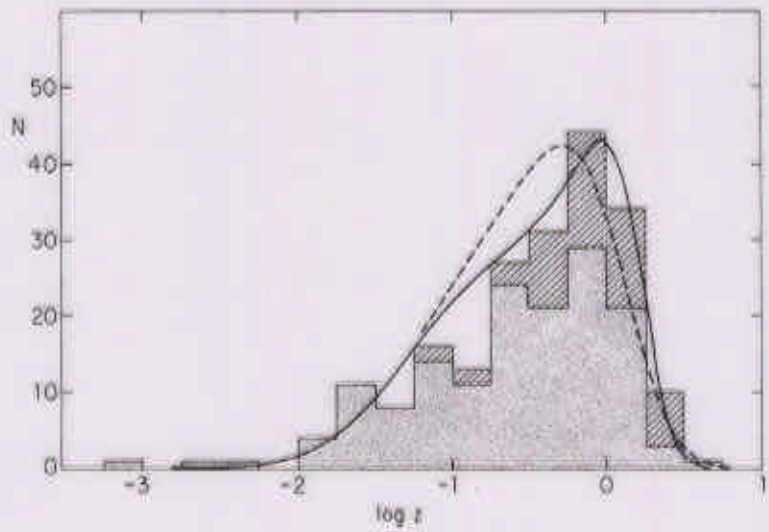

FIG. 2.—Redshift distribution of 202 sources stronger than $S = 2$ Jy at 1.4 GHz in $\omega = 3.86$ sr. Sources with spectroscopic redshifts are represented by the stippled area; those with estimated redshifts, by hatching. The smooth curve is predicted by model A (§ IVa), and the broken curve by model B (§ IVb). *Abscissa*, log redshift. *Ordinate*, number of sources per bin of width 0.25 in log (z).

c) *The Local Luminosity Function*

Two forms of the luminosity function are in common use: $\rho(L, z)dL$ is the comoving density of sources at redshift z with luminosities between L and $L + dL$, and $\rho_m(L, z)d[\log_m (L)]$ is the comoving density of sources in the logarithmic luminosity range of width $d[\log_m (L)]$, where the logarithmic base m is usually 1 "magnitude" = dex (0.4). The two forms are related by

$$\rho_m(L, z) = \ln (m) L \rho(L, z) . \quad (1)$$

The "local" luminosity function $\rho_m(L, 0)$ can be obtained from radio surveys of nearby optically selected galaxies. The 1.4 GHz local luminosity function of E and S0 galaxies only has been determined by Auriemma *et al.* (1977) and is indicated by the filled circles in Figure 3. Several radio surveys of bright spiral galaxies have been made; the most sensitive at 1.4 GHz is the Westerbork survey (Hummel 1980). A $\langle V/V_m \rangle$ test is consistent with the optical sample being complete to $B_T^0 = +12.0$ (Hummel 1981) over the $\omega = 6.44$ sr solid angle defined by $\delta > -30°$ and $|b| > 20°$. The radio survey is complete above $S = 50$ mJy. The luminosity function of these galaxies was calculated by the "maximum volume," V_m, method. The maximum distance D_m at which any galaxy can be detected at both radio and optical wavelengths is the smaller of $D_r = D(S/50 \text{ mJy})^{1/2}$ and $D_o = D \text{ dex } [0.2(12.0 - B_T^0)]$, where $D = v/H_0$ is the actual galaxy distance. The corresponding $V_m = \omega D_m^3/3$. Detected galaxies were grouped in logarithmic luminosity ranges of width $m = \text{dex } (0.4)$. The portion of the local luminosity function estimated from the N spiral galaxies in each range is

$$\rho_m(L, 0) = \sum_{i=1}^{N} (1/V_m)_i , \quad (2)$$

with an rms statistical error

$$\sigma = \left[\sum_{i=1}^{N} \left(\frac{1}{V_m} \right)_i^2 \right]^{1/2} . \quad (3)$$

The results of this calculation are listed in Table 2 and plotted as open circles in Figure 3. The actual errors in $\rho_m(L, 0)$ for spirals may exceed the values σ calculated on the assumption that the galaxies are randomly distributed because most of the spirals brighter than $B_T^0 = +12.0$ and stronger than $S = 50$ mJy at 1.4 GHz lie within a volume small enough to be affected by large-scale clustering.

III. THE METHOD

The procedure used to obtain $\rho_m(L, z)$ consistent with the data is (1) set $\rho_m(L, 0)$ equal to a parametric approximation to

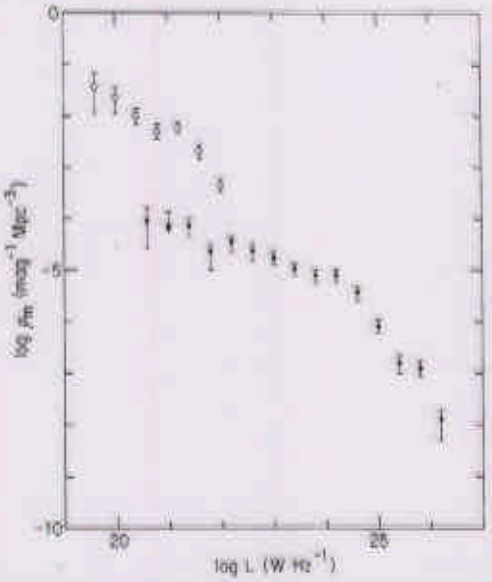

FIG. 3.—Local luminosity functions of elliptical (*filled circles*) and spiral (*open circles*) galaxies. *Abscissa*, log 1.4 GHz luminosity (W Hz^{-1}). *Ordinate*, log density per dex (0.4) luminosity interval (mag^{-1} Mpc^{-3}).

Protheroe, Biermann

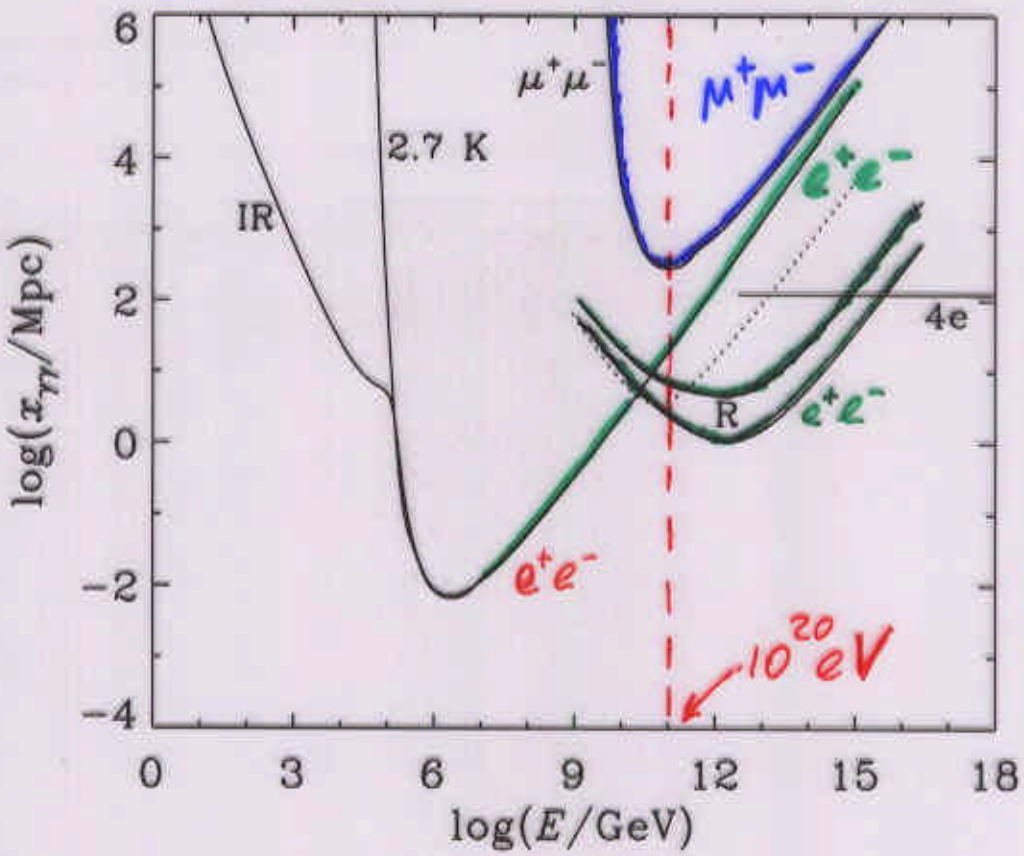

Figure 6: The mean interaction length for pair production for γ-rays in the Radio Background calculated in the present work (solid curves labelled R: upper curve – no evolution of normal galaxies; lower curve – pure luminosity evolution of normal galaxies) and in the radio background of Clark [6] (dotted line). Also shown are the mean interaction length for pair production in the microwave background (2.7K), the infrared and optical background (IR), and muon pair production ($\mu^+\mu^-$) and double pair production (4e) in the microwave background [8].

EM cascade:

pair production $\gamma\gamma_{RB} \to e^+e^-$

inverse Compton scattering $e\gamma_{CMB} \to e\gamma$

$E_\gamma \sim E_{\gamma 0} \sim \ldots$

CMB interaction length – energy attenuation

RB

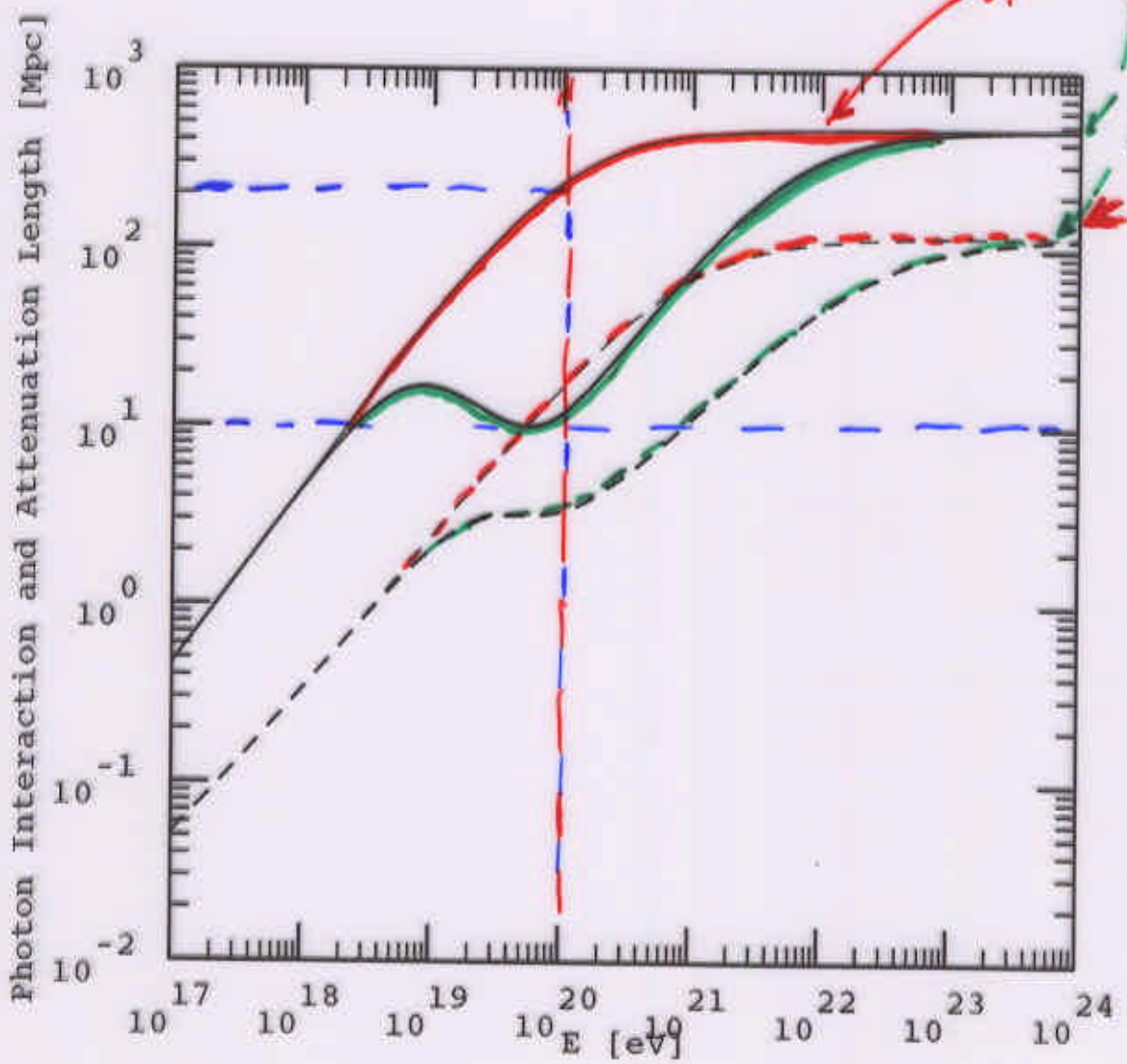

Figure 11: Interaction lengths (dashed lines) and energy attenuation lengths (solid lines) of γ−rays in the CMB (thin lines) and in the total low energy photon background spectrum shown in Fig. 5.3 with the observational URB estimate from Ref. [173] (thick lines), respectively. The interactions taken into account are single and double pair production.

$\gamma\gamma_{CMB} \to e^+e^-$ vs $\gamma\gamma_{CMB} \to \mu^+\mu^-$

Low threshold

$\sqrt{s} > 2m_e = 1$ MeV

Threshold

$\sqrt{s} > 2m_\mu = 0.21$ GeV

$E_\gamma > E_{th} = \frac{10^{20}\ eV}{1+z}$

EM cascade:

PP

$\gamma\gamma_{CMB} \to e^+e^-$

(regeneration of γ)

$e\gamma_{CMB} \to e\gamma$

ICS

Interaction length

$\lambda(\gamma\gamma \to e^+e^-)$

Energy Attenuation length:

$\lambda_{eff} \gg \lambda(\gamma \to e^+e^-)$

Muons decay

$\gamma\gamma_{CMB} \to \mu^+\mu^-$

$\mu^+ \to e^+ \nu_e \nu_\mu$

UHE νs

Interaction length

$\lambda(\gamma\gamma \to \mu^+\mu^-) \ll \lambda_{eff}$

Muons (and hence neutrinos) are produced if $\boxed{\lambda(\gamma\gamma \to \mu^+\mu^-) < \lambda_{\rm eff}}$

EM cascade $\Rightarrow$ beam of γ and e^+e^-

(definition of $\lambda_{\rm eff}$): $E_\gamma \propto \exp(-\frac{x}{\lambda_{\rm eff}})$

$\lambda_{\rm eff}$ depends on energy lost in each PP/ICS cycle: (Bonometto, '71)

$$\underline{\lambda_{\rm eff}} = \lambda(\gamma\gamma_{\rm CMB} \to e^+e^-) \times \frac{1}{m_e}\sqrt{\frac{2}{3} E_\gamma T_{\rm CMB}}$$

$$= 250 \sqrt{\frac{E_\gamma (1+z)}{10^{20}\,{\rm eV}}}\ \lambda(\gamma\gamma \to e^+e^-)$$

Compare this to $\underline{\lambda(\gamma\gamma_{\rm CMB} \to \mu^+\mu^-)}$

$$\lambda(\gamma\gamma \to \mu^+\mu^-) \approx \ln\left(\frac{m_\mu^2}{m_e^2}\right) \lambda(\gamma\gamma \to e^+e^-)$$

$$\simeq 10\ \lambda(\gamma\gamma \to e^+e^-) \ll \lambda_{\rm eff}$$

Also, for $\sqrt{s} > 0.6$ GeV (scattering is dominated by $\gamma\gamma \to e^+e^-e^+e^-$), $\lambda(\gamma\gamma \to \mu\mu) \ll \lambda_{\rm eff}$

$\lambda(\gamma\gamma_{CMB} \to \mu^+\mu^-) \ll \lambda_{eff} \Rightarrow$ photons $E_\gamma > E_{th}$ generate neutrinos

$$E_{th} = \frac{10^{20}\,eV}{1+z}$$

$\gamma\gamma_{CMB} \to \mu^+\mu^- \to e^-\bar{\nu}_e\nu_\mu$

$E_\gamma \sim 10^{20}$ eV; μ^+ slow; μ^- fast, $E_\mu \sim E_\gamma$

$E_e \sim E_\nu \sim \frac{1}{3}E_\gamma$

$e^- \to$ ICS$_{CMB}$ $\to \gamma' \to PP \to \ldots$, $E_{\gamma'} \sim \frac{1}{3}E_\gamma$

$\gamma \to \gamma' \to \gamma'' \Rightarrow E_{\gamma''} \sim 10^{-1}E_\gamma$

Two rounds of μ-PP reduce energy below threshold

$\Rightarrow \simeq 4$ energetic neutrinos per photon

In fact, more: $\gamma\gamma \to \pi^+\pi^-$ also contribute

Flux and energy of neutrinos

Sources (TD, relic particles, etc.) produce photons at some rate: $\dot{n}_X$

Evolution of the source: $\dot{n}_X = \dot{n}_{X,0}\left(\frac{t}{t_0}\right)^{-m}$

Neutrino flux: 2ξ ν's per γ

$$n_\nu = 2\xi \int_{z_R}^{z_{max}} dt\ \dot{n}_X (1+z)^{-4} =$$

$$= \frac{3}{2a} 2\xi\, \dot{n}_{X,0}\, t_0 \left[(1+z_R)^a - (1+z_{max})^a\right]$$

$a = \frac{3m-11}{2}$, $z_{max} \approx 3\cdot 10^3$ for $E_\nu \sim 10^{17}$–10^{18} eV

Gelmini, Gondolo, Sarkar

Photons with $E_\gamma > E_{th} = \frac{10^{20}\,eV}{1+z}$ produce neutrinos.

At $z<1$ photons from these sources reach us from closer than 10 Mpc $\Rightarrow z < 0.002 \equiv z_{GZK,\gamma}$

These fluxes are related:

$$n_\nu = 2\xi\, \underbrace{n_{\gamma,0}\left(E_\gamma > \frac{10^{20}\,eV}{1+z_R}\right)}\ \frac{(1+z_R)^a - (1+z_{max})^a}{1-(1+z_{GZK,\gamma})^a}$$

$$= \xi\, n_\gamma (E > E_{GZK}) = J\,\varphi_{GZK};\quad \text{Ch. 3-10}$$

$$\varphi_\nu = 2\xi S\, n_{CR}(E>E_{GZK})\, \frac{(1+z_R)^a - (1+z_{max})^a}{1-(1+z_{GZK,\delta})^a}$$

m = 3 (TD: ordinary strings, monopolonium, ...)

$a = -1 < 0 \Rightarrow$ flux dominated by contribution from $z \sim z_R$

Neutrino energy $E_\nu \simeq \frac{E_M}{3} \simeq \frac{E_{th}}{3(1+z)}$

$$\simeq \frac{3\times 10^{19}\ eV}{(1+z_R)^2} \sim 10^{18}\ eV$$

m ≥ 4 (Superconducting strings, etc.)

$a > 0 \Rightarrow$ flux dominated by $z \sim z_{max}$

Neutrino energy: $E_\nu \sim 10^{11} - 10^{17}\ eV$

$\sqrt{s_{\gamma\gamma}} \sim 3$-$10$ GeV $\Rightarrow$ $\gamma\gamma_{CMB} \to \pi^+\pi^-$

$\to \pi^+\pi^-\pi^+\pi^-$

$\Rightarrow$ more neutrinos per photon

Predicted flux:

$$\varphi_\nu \approx \begin{cases} 10^{-20}\ \mathrm{cm^{-2}s^{-1}sr^{-1}}, & m=0 \leftarrow \text{very small} \\ 3\times10^{-16}\ \mathrm{cm^{-2}s^{-1}sr^{-1}}, & m=3 \leftarrow \text{can detect soon!} \\ > 10^{-13}\ \mathrm{cm^{-2}s^{-1}sr^{-1}}, & m\geq 4 \leftarrow \text{exceeds upper limit from Fly's Eye (HiRes)} \end{cases}$$


m=4


m=3

2 NEUTRINO FLUX PREDICTIONS

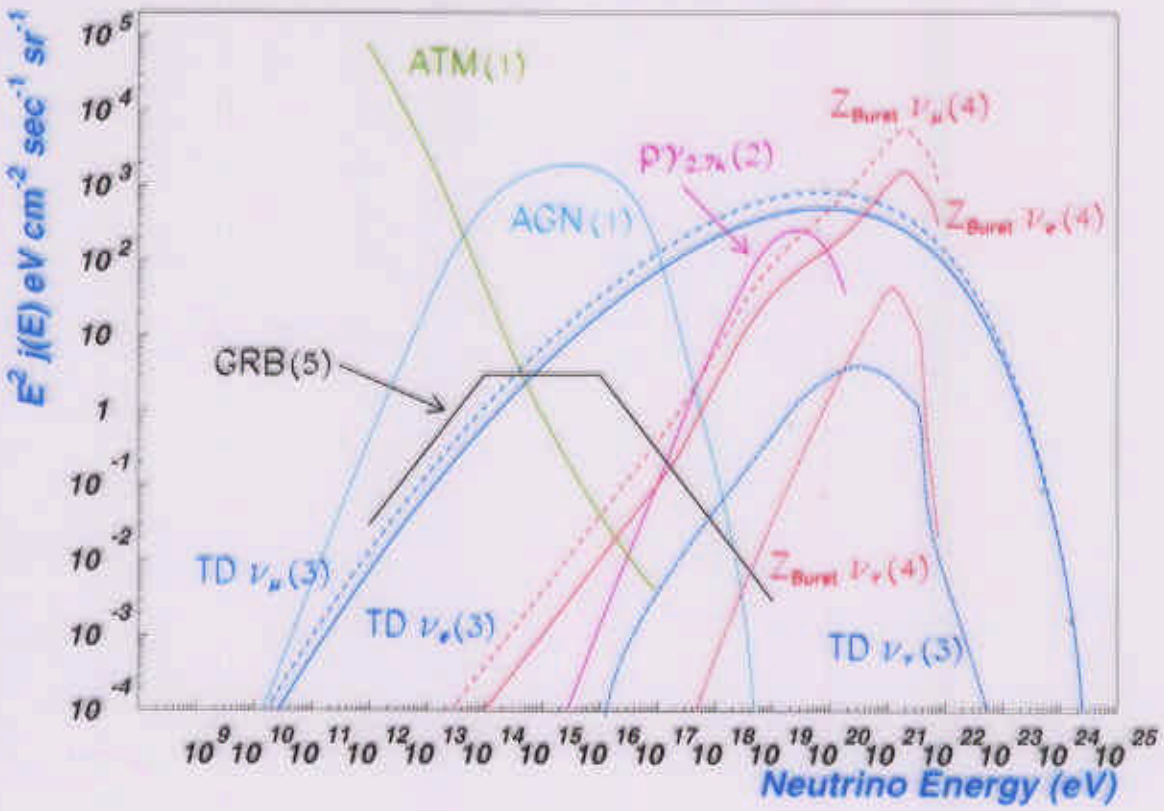

Figure 1: Neutrino flux predictions: Atmospheric and AGN (1: Stecker & Salamon 1996, Space Sci Rev 75, 341), photomeson production via $p\gamma_{2.7K}$ (2: Stecker, Done, Salamon, & Sommers 1991, Phys. Rev. Letters 66, 2697), topological defects (3: Sigl, Lee, Bhattacharjee, & Yoshida 1998, Phys. Rev. D 59, 043504), $m_X = 10^{16}$ GeV, X $\Rightarrow$ q + q, supersymmetric fragmention), Z_{Burst} (4: Yoshida, Sigl, & Lee 1998, Phys. Rev. Letters 81, 5055), $m_\nu = 1$ eV, Primary $\Phi_\nu \sim E^{-1}$), and gamma ray bursts (5: Waxman & Bahcall 1997, Phys. Rev. Letters 78, 2292).

Figure 1 illustrates the high energy neutrino flux predictions from various astrophysical sources as a function of neutrino energy. Note that curves show the differential neutrino flux multiplied by E_ν^2 which is equivalent to an energy flux. In the energy range of $10^{14} to 10^{17}$ eV, the AGN neutrino flux is predicted to dominate over other sources. However, neutrinos from individual gamma-ray bursts may be observable via their directionality and short, intense time characteristics. The time-averaged

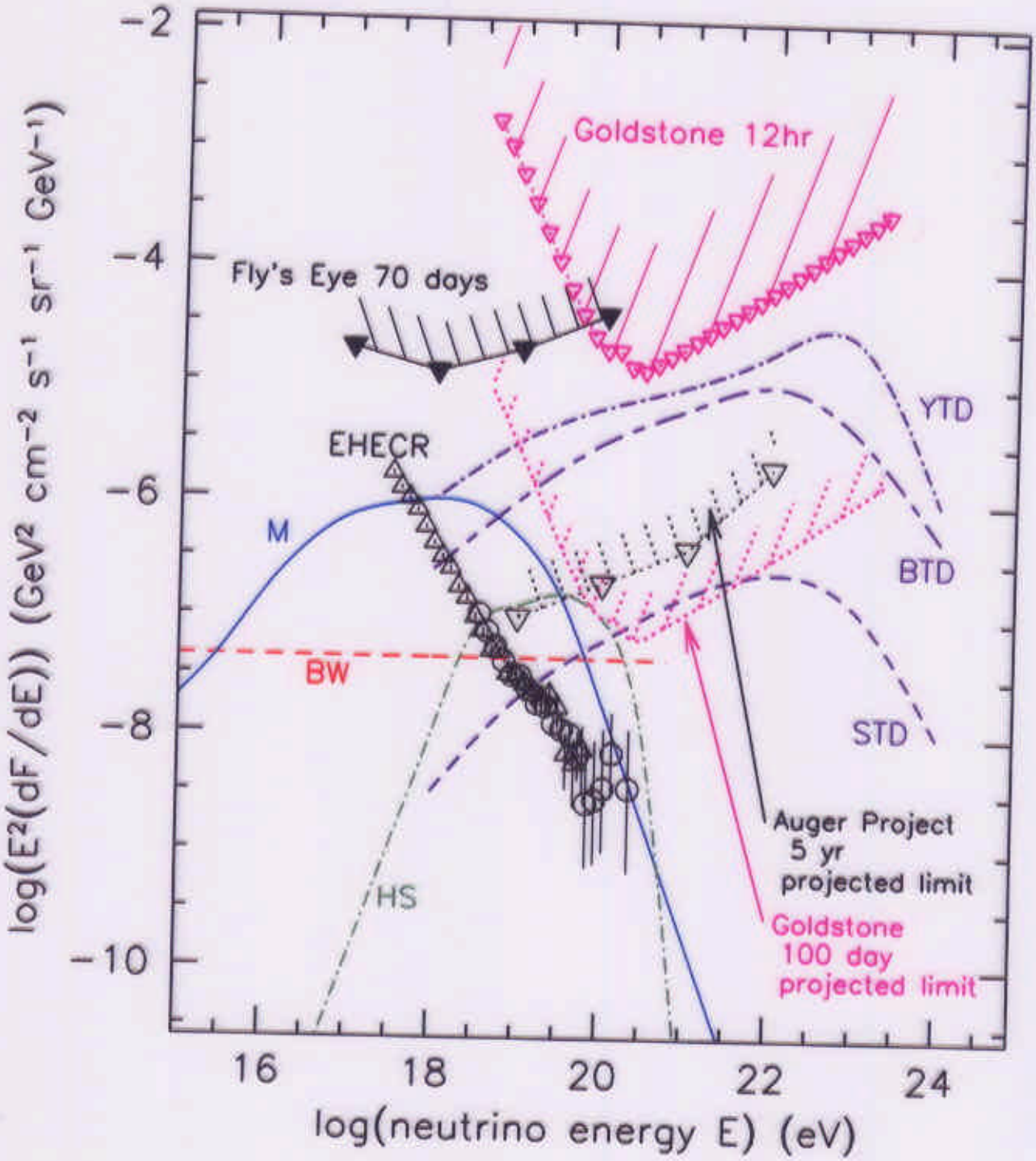
Goldstone 12hr
Fly's Eye 70 days
YTD
EHECR
M
BTD
BW
STD
Auger Project
5 yr
projected limit
HS
Goldstone
100 day
projected limit
−2
−4
−6
−8
−10
16
18
20
22
24
log(E²(dF/dE)) (GeV² cm⁻² s⁻¹ sr⁻¹ GeV⁻¹)
log(neutrino energy E) (eV)

Conclusion

- Sources of UHE photons (TDs, relic particles, etc.) that operate at $z \gtrsim 3$ produce neutrinos with energy $E_\nu \sim 10^{18}$ eV

- Flux depends on evolution index m of the source

  $m = 3$ (TD: strings, monopolonium) $\Rightarrow$ can soon detect

  $m \geq 4$ (TD: supercond. strings) $\Rightarrow$ already ruled out